

Vertical deformation and sea level changes in the coast of Chile by satellite altimetry and tide gauges

Henry D. C. Montecino, Vagner G. Ferreira, Aharon Cuevas, Leoncio Castro Cabrera, Juan Carlos Soto Báez & Silvio R. C. De Freitas

To cite this article: Henry D. C. Montecino, Vagner G. Ferreira, Aharon Cuevas, Leoncio Castro Cabrera, Juan Carlos Soto Báez & Silvio R. C. De Freitas (2017) Vertical deformation and sea level changes in the coast of Chile by satellite altimetry and tide gauges, International Journal of Remote Sensing, 38:24, 7551-7565, DOI: [10.1080/01431161.2017.1288306](https://doi.org/10.1080/01431161.2017.1288306)

To link to this article: <https://doi.org/10.1080/01431161.2017.1288306>



Published online: 14 Feb 2017.



Submit your article to this journal [↗](#)



Article views: 226



View related articles [↗](#)



View Crossmark data [↗](#)



Citing articles: 1 View citing articles [↗](#)



Vertical deformation and sea level changes in the coast of Chile by satellite altimetry and tide gauges

Henry D. C. Montecino^{a,b}, Vagner G. Ferreira^c, Aharon Cuevas^a,
Leoncio Castro Cabrera^a, Juan Carlos Soto Báez^d and Silvio R. C. De Freitas^b

^aDepartment of Geodetic Sciences and Geomatics, University of Concepción, Los Angeles, Chile; ^bGeodetic Sciences Graduation Course, Federal University of Paraná, Curitiba, Brazil; ^cSchool of Earth Sciences and Engineering, Hohai University, Nanjing, China; ^dNational Seismological Centre, University of Chile, Santiago, Chile

ABSTRACT

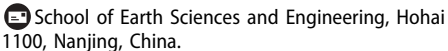
Located at the intersection of the triple junction between the Nazca, South American, and Antarctic plates, the Chilean territory is subject to active lithospheric deformations and seismicity. Taking the difference between the satellite altimetry (ALT) data that give the absolute sea level variation and the tide gauge (TG) observations that record the relative sea level variation, we computed the absolute vertical crustal motion of the TG sites. We used 11 TG stations along the Chilean coast and altimeter measurements from multi-satellite missions (Topex, Jason-1 (A), and Jason-2) in nearby waters. The ALT-TG vertical deformations were compared with trends obtained from GPS measurements, which showed good consistency in terms of a correlation coefficient of about 0.9 (in 8 of 11 stations). Our results reveal that the behaviour of the long-term vertical deformations along the Chilean coast presented an important spatial variability. We also estimated the sea level change (SLC) through a multivariate model involving linear trend and decadal and inter-decadal climatic influence; in addition, the glacial isostatic adjustment effect was also removed. Our estimation of the SLC in the Chilean coast revealed an overall increase in sea level. The sea level in Chile does not strictly follow the global trend of the past two decades ($\sim 3 \text{ mm year}^{-1}$), but rather a slight agreement (from 1.2 to 0.6 mm year^{-1}) from Arica up to Puerto Montt approximately, with the exception of PTAR and PWIL TGs, where we found a decrease of -0.9 and $-0.8 \text{ mm year}^{-1}$, respectively.

ARTICLE HISTORY

Received 24 August 2016
Accepted 23 January 2017

1. Introduction

The structural tectonic features in the Chilean region are particularly important for global geodynamical studies. These are mainly due to the triple junction plates in the region, with the intersection of the Nazca and South American plates in most of the country's area, and the Antarctic plate in the far south. This interaction between tectonic plates make the region subject to frequent and strong earthquakes, as well as tsunamis and volcanism (see Vigny et al. 2011; Gusman et al. 2015; Watt, Pyle, and Mather 2009).

CONTACT Vagner G. Ferreira  vagnergf@hhu.edu.cn 

© 2017 Informa UK Limited, trading as Taylor & Francis Group

These phenomena cause deformations in the crust of the Earth. The related information is fundamental in understanding the interior process of the Earth, which is typically explored through geophysical inversion. Because the interplate convergence zone generated by the Nazca and South American plates is along the continental margin, it is important to study the long-term vertical deformation in the Chilean ocean–continent interface. In addition, the vertical land motion could contribute to studies of other processes, such as: the secular sea level change (SLC) (Snay et al. 2007), glacial isostatic adjustment (GIA) effect (Milne et al. 2001), volcanic activity (Sturkell et al. 2006), and subsidence due to both natural and anthropogenic induced changes (Bawden et al. 2001).

A large number of geodynamic studies based on crustal deformations are done by using geodetic space based techniques, mainly by the facilities in referring and comparing observations in a consistent global geodetic reference frame (GRS). In this context, observations are typically derived from GPS (Beavan et al. 2010; Larson and Van Dam 2000), as well as by satellite laser ranging – SLR (Noomen et al. 1996), Doppler orbitography and radiopositioning integrated by satellite – DORIS (Soudarin, Crétaux, and Cazenave 1999), interferometric synthetic aperture radar – InSAR (Dalla Via, Crosetto, and Crippa 2012), and very long baseline interferometry – VLBI (Tesmer et al. 2009). Most of the crustal deformation studies are based on Global Navigation Satellite System (GNSS) observations due to high levels of accuracy and moderate associated costs, in order to achieve a broad spatial coverage in relation to SLR and VLBI techniques (Blewitt 2007) or the other named techniques.

However, in South America, particularly Chile, a dense, long-term time series and homogenous GNSS network along the Chilean coast does not currently exist. Although velocity models of the Earth's crust exist, such as velocity model – VeMos, they have few stations in the study region, do not involve the vertical component or have short periods of observation (Drewes and Heidbach 2012; Sánchez and Drewes 2016). Consequently, studying geodynamic phenomena from long-term time series presents difficulties. Thus, other alternatives are necessary. Satellite altimetry (ALT) and tide gauge (TG) records provide alternative and independent methods for estimating vertical land motion (Fenoglio-Marc, Dietz, and Groten 2004; Nerem 2002; Cazenave et al. 1999). In long records of TG data (e.g. >20 years), vertical deformations from ALT and TG could be complementary to the poor density present in continuous GNSS station network.

In this study, we used a TG time series belonging to the Chilean Tide Gauge Network (CHTGN) and a time series from multi-mission (Topex, Jason-1, and Jason-2) satellite ALT between January 1994 and January 2015 (~20 years). The sea level measured by ALT is relative to the geocentre, and is, therefore, independent from vertical land motion. The sea level measured by a TG station is relative to the Earth's crust. For this reason, the vertical land motion is contained in the long-term time series of the difference between the ALT and TG sea level height measurements (indicated here as ALT-TG).

We used ALT data to estimate vertical crustal motion. We considered the behaviour of the regional SLC in the Chilean coast. Chile has a long coastline; hence, the understanding of the behaviour in SLC and its relationship with the global trend is fundamental to projecting and adapting the infrastructure and dynamics of economic and cultural activities.

Research has shown that in the last two decades, the global SLC in open oceans is $\sim 3 \text{ mm year}^{-1}$ (Church et al. 2013; Cazenave and Nerem 2004; Lombard et al. 2005; Nerem et al. 2010), albeit at the coast it is only $2.4 \pm 0.1 \text{ mm year}^{-1}$ (Prandi, Cazenave, and Becker 2009). Nevertheless, the SLC in regional terms may show disagreement regarding the global trend, including numbers up to 10 times greater than the global mean, and other regions exhibiting an inverted trend showing negative variations of up to 15 mm year^{-1} (Church et al. 2010; Melini and Piersanti 2006). These changes may be the result of regional climate variability on different time scales. For example, the El Niño Southern Oscillation (ENSO) is a key source of inter-annual variability. This variability in the Pacific has a decadal or inter-decadal pattern; these phenomena are known as Pacific decadal oscillation (PDO) and inter-decadal Pacific oscillation (IPO), respectively.

In this article, we estimated vertical deformations from 11 TGs and altimeter multi-mission measurements along the Chilean coast, and made a comparison with vertical motion from GPS positioning. In addition, we have presented an analysis of the coastal SLC based on a simple linear regression and multi-variable linear regression model.

2. Data and methods

2.1. Satellite ALT time series

We used satellite ALT data from different missions in order to cover a period of approximately 20 years. The satellite ALT data used are shown in Table 1.

The ALT data were obtained from The Radar Altimeter Database System (RADS), from the Department of Earth Observation and Space Systems of the Engineering, Faculty of Aerospace, from Delft University of Technology (DEOS 2015). The satellite ALT observations have been corrected for delays caused by atmospheric refraction, the sea state bias and the tides, as summarized in Table 2 (Fenoglio-Marc, Dietz, and Groten 2004). The data used consist of the sea level anomalies (SLA), defined as the difference between the geocentric sea surface height, and an available world-wide validated global geopotential model with height spectral resolution and low commission errors, so the EGM2008 (Pavlis et al. 2012) is considered to generate the global geoid used as a vertical reference surface.

We interpolated the ALT measurements to each TG location. To do this, the ALT data were convolved with a two-dimensional (2D) Gaussian function centred at the TG location. The function takes the value 1/2 at a distance of 50 km from the TG and vanishes beyond 500 km (cf. García et al. 2012; Wahr, Molenaar, and Bryan 1998). Furthermore, we did not correct the ALT data for the inverse barometric effect, because we did not apply this correction to the TG data.

Table 1. Satellite altimetry data used.

Mission	Period	Cycles
Topex	25 September 1992–11 August 2002	001–364
Jason-1 (A)	15 January 2002–26 January 2009	001–260
Jason-2	4 July 2008–6 January 2015	000–240

Table 2. Corrections applied to the altimetric signal in Topex, Jason-1 (A), Jason-2, Envisat missions (DEOS 2015).

Correction/mission	Topex	Jason-1 (A)	Jason-2
Orbit	GSFC GDR-C Prime orbital altitude	ESOC EIGEN-6 C orbital altitude	GSFC/std1204 orbital altitude
Dry tropospheric correction	ECMWF dry tropospheric correction	ECMWF dry tropospheric correction	ECMWF dry tropospheric correction
Wet tropospheric correction	ECMWF model wet tropospheric correction	ECMWF model wet tropospheric correction	ECMWF model wet tropospheric correction
Ionospheric correction	Dual-frequency ionospheric correction	Dual-frequency ionospheric correction	Dual-frequency ionospheric correction
Inverse barometric correction	None	None	None
Solid earth tide	Solid earth tide	Solid earth tide	Solid earth tide
Ocean tide	GOT 4.9 ocean tide	GOT 4.8 ocean tide	GOT 4.8 ocean tide
Load tide	GOT 4.8 load tide	GOT 4.8 load tide	GOT 4.8 load tide
Pole tide	Pole tide	Pole tide	Pole tide
Sea state bias	CLS sea state bias	CLS non-parametric sea state bias	CLS non-parametric sea state bias
Reference surface	EGM2008 geoid height	EGM2008 geoid height	EGM2008 geoid height
Reference frame offset	Reference frame offset	Reference frame offset	Reference frame offset

In order to correct the bias between altimeter missions and estimate the trend and oscillation cycles simultaneously in the same mathematical model, we applied a trajectory model (cf. Bevis and Brown 2014), the sea surface anomaly (*ssa*) in the epoch t can be written as

$$\begin{aligned}
 ssa(\varphi, \lambda, t) = & ssa(\varphi, \lambda, t_0) + m_i(t - t_0) + \sum_{j=1}^{n_j} \text{bia } s_j H(t - t_j) \\
 & + \sum_{k=1}^2 [A_k \cos(2\pi\omega_k t) + B_k \sin(2\pi\omega_k t)], \quad (1)
 \end{aligned}$$

where φ, λ are the geodetic coordinates, t_0 is the origin epoch of the time series, t is the actual epoch, c is a constant, m is the trend, bia_j is the bias term in the epoch j , n_j is the number of bias (the altimeter missions linked to Equation (1) are equal to n_j+1), H is the Heaviside function and A_k and B_k are parameters containing information about the amplitudes (R) and phases (φ), and k provides the annual ($k = 1$) and semi-annual ($k = 2$) components. Once the bias was estimated, all data from each altimeter time series were linked to the same reference.

The ALT time series showed an average trend of 0.2 mm year^{-1} with an average standard deviation of $\pm 4.2 \text{ mm year}^{-1}$, and a maximum trend of 4.1 and 0.7 mm year^{-1} for TGs and ALT, respectively.

The annual and semi-annual amplitudes from the ALT time series present a significant spatial variability. In addition, they have an inverse spatial pattern, that is, the annual amplitude decreases from north to south, while the semi-annual amplitude increases from north to south. The average values for the annual and semi-annual amplitude are 27.7 and 9.4 mm , respectively (see Table 4).

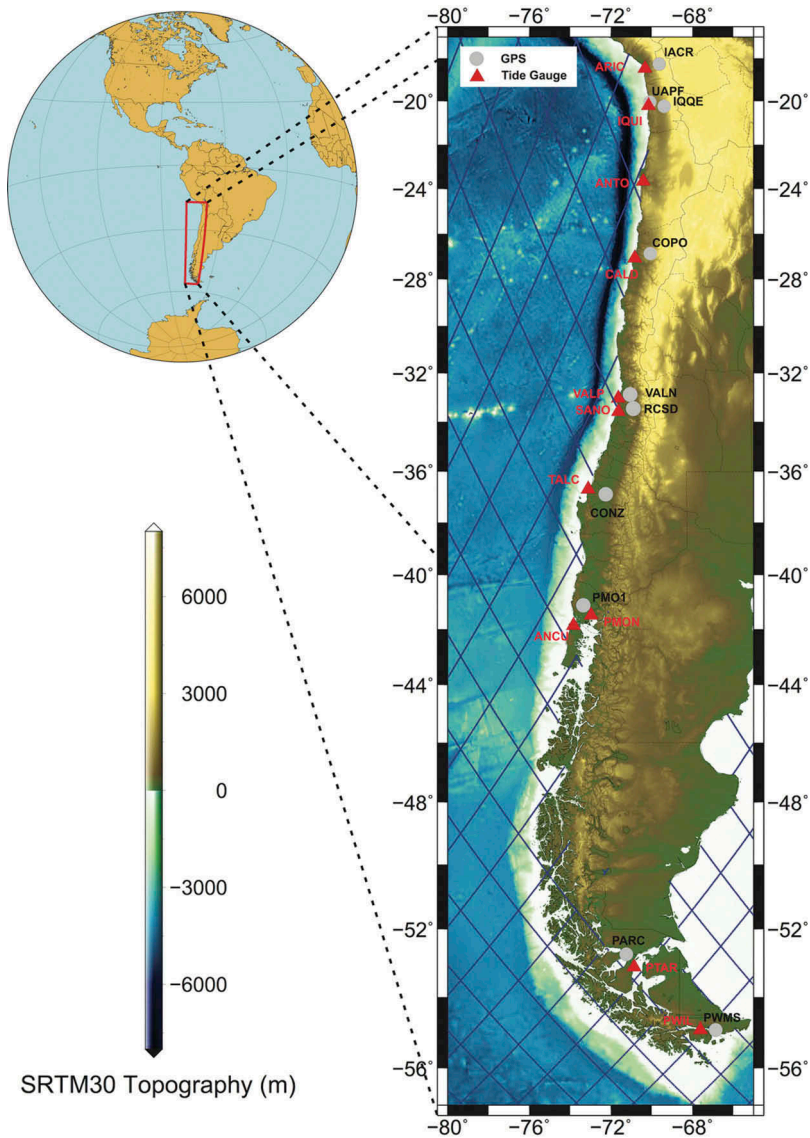


Figure 1. Study region. The TGs, ALT tracks crossovers and GPS stations are displayed, respectively, by red, green, and grey dots.

2.2. TG time series

A set of 11 TGs were selected with monthly data recorded for around 20 years covering the time-span of January 1994–January 2015 along the Chilean coast. The TG observations were provided by the Hydrographic and Oceanographic Service of the Chilean Navy – SHOA (see Figure 1).

We calculated the TG time series in terms of SLC with regards to first sea level value. In addition, we removed the gross errors according to the 3σ rule.

In order to determine a mean linear trend, we fitted the observations by using a least square approximation with a sequence $y(t)$ composed of a linear function and annual and semi-annual oscillations:

$$y(t) = a_0 + a_1(t) + \sum_{k=1}^2 [A_k \cos(2\pi\omega_k t) + B_k \sin(2\pi\omega_k t)], \quad (2)$$

where t is the epoch, a_0 is a constant term, a_1 is the linear trend, A_k and B_k are parameters containing information about the amplitudes (R) and phases (φ), and k provides the annual ($k = 1$) and semi-annual ($k = 2$) components. The parameters were estimated by a least squares adjustment and are presented in Table 3.

The parameters estimated from Equation (2) to TGs showed an average trend of $-0.4 \text{ mm year}^{-1}$ with a standard deviation of $\pm 0.8 \text{ mm year}^{-1}$.

In other words, the trends in TG and ALT time series present magnitudes as signs varied along the Chilean coast, reaching a significant degree of dispersion reflected in the value of its standard deviation (see Table 4).

The annual and semi-annual amplitudes showed significant spatial variability. On average, the annual and semi-annual amplitudes reach 38.3 and 18.8 mm, respectively. In the annual amplitudes, an average of differences of $\sim 10 \text{ mm}$ can be observed between TG and ALT and a low correlation (correlation coefficient: -0.2); however, large differences were obtained in the semi-annual amplitudes, and the TG semi-annual amplitudes were, on average, almost double those of the ALT. Nevertheless, semi-annual amplitudes of TG and ALT presented a high correlation (correlation coefficient: 0.9). Regarding the annual amplitude, no pattern was observed in the signal. However, in the semi-annual amplitude, an increase in a north to south direction was observed.

On the other hand, the annual and semi-annual phases of both TG and ALT sensors presented great spatial variability, without identifying a predominant pattern. In addition, the differences between the phases obtained from TG and ALT presented significant discrepancies, reaching maximum differences of ~ 9 (-285°) and ~ 6 (188°) months for annual and semi-annual amplitudes, respectively (see Table 4). We believe that these differences can be explained by a number of causes, including: deficiency in the interpolation of altimeter measurements, meteorological, and oceanographic regional

Table 3. Trends, amplitudes, and phases of the TG time series.

Station	Parameter					Standard deviation				
	$a_1 \text{ (mm year}^{-1}\text{)}$	$R_1 \text{ (mm)}$	$R_2 \text{ (mm)}$	$\varphi_1 \text{ (}^\circ\text{)}$	$\varphi_2 \text{ (}^\circ\text{)}$	$a_1 \text{ (mm year}^{-1}\text{)}$	$R_1 \text{ (mm)}$	$R_2 \text{ (mm)}$	$\varphi_1 \text{ (}^\circ\text{)}$	$\varphi_2 \text{ (}^\circ\text{)}$
ARIC	3.3	44.8	8.5	92.2	-31.9	0.5	4.4	4.5	5.8	30.2
IQUI	-2.3	28.4	8.2	91.9	-21.2	0.6	5.2	5.2	10.5	36.3
ANTO	0.3	35.8	6.2	75.4	38.5	0.6	4.9	5.0	8.0	45.9
CALD	-3.1	35.8	7.2	94.2	23.1	0.6	4.5	4.5	7.3	36.0
VALP	-2.8	20.1	10.5	84.9	6.4	0.6	5.0	5.2	14.8	27.8
SANO	1.0	38.6	16.8	76.1	36.2	0.7	6.1	6.1	9.2	20.9
TALC	-5.2	37.6	26.4	151.9	40.6	0.6	5.3	5.3	8.1	11.5
PMON	3.0	28.9	22.3	156.9	41.8	0.7	6.5	6.4	12.7	16.6
ANCU	-2.4	69.1	25.4	-171.1	28.5	1.1	7.4	7.4	6.1	16.4
PTAR	-0.7	28.2	40.8	115.2	-13.7	1.0	9.2	9.3	18.8	12.7
PWIL	4.1	53.7	35.1	81.7	-5.5	1.2	10.8	10.8	11.4	17.4

Bias between Topex Jason-1 and between Jason-1 and Jason-2 of the ALT time series.

Table 4. Trends, amplitudes, and phases of the ALT time series.

Station	Parameter						Standard deviation							
	α_1 (mm year ⁻¹)	bias ₁ (mm)	bias ₂ (mm)	R_1 (mm)	R_2 (mm)	φ_1 (°)	φ_2 (°)	α_1 (mm year ⁻¹)	bias ₁ (mm)	bias ₂ (mm)	R_1 (mm)	R_2 (mm)	φ_1 (°)	φ_2 (°)
ARIC	0.7	30.0	-33.8	35.7	5.4	28.4	71.4	3.1	0.4	4.2	4.0	1.4	2.4	15.0
IQUI	0.5	45.8	-49.2	35.4	6.9	22.7	152.6	2.8	0.4	3.8	3.6	1.3	2.2	10.5
ANTO	0.5	35.5	-37.1	33.4	4.4	49.1	93.6	2.8	0.3	3.6	3.3	1.2	2.5	15.8
SANO	0.6	16.7	9.6	26.3	6.5	79.5	-59.0	4.1	0.5	4.9	4.2	1.6	5.4	14.6
CALD	0.0	-0.1	7.2	29.8	6.1	81.9	24.5	3.5	0.4	4.5	3.9	1.5	4.5	14.3
VALP	0.6	18.0	8.1	26.8	6.8	80.2	-79.7	4.0	0.5	4.9	4.2	1.6	5.3	13.8
TALC	0.2	77.4	-37.5	26.5	9.2	93.7	-111.1	4.9	0.6	5.9	4.9	2.0	7.0	12.4
PMON	0.6	64.2	-21.1	26.0	11.0	110.4	-160.1	4.4	0.5	5.7	4.5	1.9	7.6	9.8
ANCU	0.5	64.8	-21.3	26.4	11.0	114.2	-160.0	4.4	0.5	5.7	4.4	1.9	7.6	9.8
PTAR	-1.1	77.1	15.3	20.4	18.1	112.1	166.6	5.9	0.7	7.2	5.7	2.4	12.3	7.5
PWIL	-1.0	62.3	24.1	18.1	18.1	108.9	158.9	6.5	0.7	7.7	6.0	2.5	14.4	8.0

Table 5. Sea level trends obtained from TG and altimetry and vertical deformation.

TG	φ (°)	\dot{t}_g (mm year ⁻¹)	s_a (mm year ⁻¹)	u (mm year ⁻¹)
ARIC	-18.47975	3.3 ± 0.5	0.7 ± 3.1	-2.6 ± 3.1
IQUI	-20.27354	-2.3 ± 0.6	0.5 ± 2.8	2.8 ± 2.9
ANTO	-23.65305	0.3 ± 0.6	0.5 ± 2.8	0.2 ± 2.9
SANO	-33.65400	1.0 ± 0.7	0.6 ± 4.1	-0.4 ± 4.2
CALD	-27.06444	-3.1 ± 0.6	0.0 ± 3.5	3.1 ± 3.6
VALP	-33.02724	-2.8 ± 0.6	0.6 ± 4.0	3.4 ± 4.0
TALC	-36.84377	-5.2 ± 0.6	0.2 ± 4.9	5.4 ± 4.9
PMON	-41.46900	3.0 ± 0.7	0.6 ± 4.4	-2.4 ± 4.5
ANCU	-41.86694	-2.4 ± 1.1	0.5 ± 4.4	2.9 ± 4.5
PTAR	-53.13695	-0.7 ± 1.0	-1.1 ± 5.9	-0.4 ± 6.0
PWIL	-54.93333	4.1 ± 1.2	-1.0 ± 6.5	-5.1 ± 6.6

factors, and of the different state of the sea level observed in open ocean by altimeter, and on the coast by the TG (see Table 5).

2.3. GPS time series

GPS positioning is currently a widely used technique in geoscience for the estimation of geocentric coordinates. In order to evaluate the performance of vertical deformations obtained from ALT data and TG records, we performed a comparison with the deformations obtained from eleven continuous GPS stations.

The GPS stations contain data obtained during the study period (2008–2015) with records from 4 to 8 years, which is shorter than the vertical motion referred to in Section 3.1. The GPS data processing was carried out with the Bernese 5.2™ software, and the estimation of coordinates was based on the latest strategies and models in GPS processing. The Wet & Dry mapping function was used (Niell 1996), as well as absolute phase center antenna correction (Schmid et al. 2007). The GPS time series used refer only to the up component.

On 17 April 2011, International GNSS Service (IGS) made a GRS transition used as a reference for orbits from IGS05 to IGS08. A change in the coordinates was expected, however, we performed a transformation from IGS08 to IGS05 based on the T_x , T_y , and T_z parameters (Rebischung et al. 2012), and variations in height by IGS change did not exceed 1 mm. In addition, the errors of our GPS time series fluctuated around 1.5 mm; therefore, this effect is considered negligible in our study.

In order to homogenize the GPS time series with ALT and TGs, the systematic effect (e.g. antenna change) that occurred during the study period (see Table 6) was removed from the GPS time series using the trajectory model (cf. Equation (1)). The jump term of the model used was estimated in the epochs where there was an earthquake or an antenna, receiver or firmware change, as published in the US Geological Survey website. In addition, before estimating the trend in the GPS time series, the 3σ rule was applied to remove outliers.

2.4. Vertical deformation from ALT-TG and SLC

The geocentric vertical motion of the coast (\dot{u}) is linked to the rate of vertical SLC relative to the Earth's crust (\dot{t}_g) measured by the TG, and to the rate of geocentric SLC (\dot{s}_a) measured by ALT, through the relationship (Nerem 2002):

Table 6. Vertical motion from TG/ALT and GPS positioning.

TG	GPS	Period	u (mm year ⁻¹)	u_{GPS} (mm year ⁻¹)
ARIC	IACR	January 2012–April 2015	-2.6 ± 3.1	-2.7 ± 0.4
IQUI	UAPF	January 2000–January 2004	2.8 ± 2.9	2.5 ± 0.7
ANTO	IQQE	May 2008– January 2015	0.2 ± 2.9	2.6 ± 0.2
SANO	RCSO	August 2008.8–January 2015	-0.4 ± 4.2	0.3 ± 0.6
CALD	COPO	May 2012–May 2015	3.1 ± 3.6	8.9 ± 0.7
VALP	VALN	January 2007–January 2015	3.4 ± 4.0	-4.7 ± 0.2
TALC	CONZ	January 2007– January 2015	5.4 ± 4.9	-5.8 ± 0.4
PMON	PMO1	September 2007–January 2015	-2.4 ± 4.5	4.1 ± 0.2
ANCU	PMO1	September 2007–January 2015	2.9 ± 4.5	4.1 ± 0.2
PTAR	PARC	January 2007–January 2015	-0.4 ± 6.0	-1.8 ± 0.2
PWIL	PWMS	February 2010–April 2015	-5.1 ± 6.6	-3.4 ± 0.2

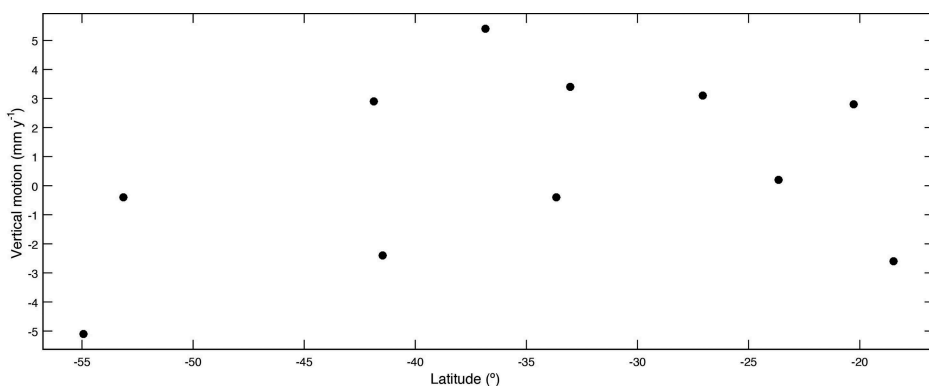
$$\dot{u}(\varphi, \lambda) = \dot{s}_a(\varphi, \lambda) - \dot{t}_g(\varphi, \lambda), \quad (3)$$

where φ and λ are the geodetic latitude and longitude, respectively.

The rate of geocentric SLC \dot{s}_a measured by satellite ALT in the period January 1994–January 2015 was evaluated at each TG location. This was realized through a least squares procedure by solving the linear-term of the time-series based on the monthly average ALT SLA.

Absolute SLC can also be estimated from TG records corrected from vertical movements, such as those obtained from GNSS positioning. However, in our case there were few and short observation periods for GNSS stations, so our estimate is based on ALT data.

In order to determine the SLC between January 1994 and January 2015, we estimated the trend from a Multivariate Linear Regression model (MVLRL). In the MVLRL, in addition to the contents in the linear trend in sea level over time, also models the decadal climate index (DCI) designed as δ_{DCI} , and the inter-decadal climate index (ICI) designed as δ_{ICI} variables. The δ_{DCI} and the δ_{ICI} represent the decadal and inter-decadal variability in the Pacific. The δ_{DCI} was obtained from a low-pass filter (with a 10 year window) PDO, obtained from <http://research.jisao.washington.edu/pdo/PDO.latest>. The δ_{DCI} was estimated from the high-pass filtering multivariate ENSO index (MEI), and obtained from <http://www.esrl.noaa.gov/psd/ens/mei/table.html> (see Figure 2). The MEI represents

**Figure 2.** Vertical deformation behaviour of the Chilean coast from north to south.

the El Niño Southern Oscillation (ENSO), but is defined based on six main observed atmospheric and oceanic variables over the tropical Pacific that are closely related to ENSO events (Wolter and Timlin 1998).

Thus, the multivariate model used to separately identify annual, decadal, and longer term trends was (Zhang and Church 2012):

$$\hat{\eta}(t) = b_0 + b_1t + b_2\delta_{\text{DCI}}(t) + b_3\delta_{\text{ICI}}(t) + \varepsilon_0(t), \quad (4)$$

where b_0 is the intercept, b_1 is the sea level linear trend, b_2 is regression with respect to the δ_{DCI} (i.e. the low-passed PDO index), b_3 is regression with respect to the δ_{ICI} (i.e. the high-passed MEI index), t is the epoch, and ε_0 is the error. The parameters in Equation (4) were solved by least square adjustment. Additionally, the vertical deformation influenced by the Earth's overall response to changes in load ice after the last glacial period (GIA) was removed by a global model. Noteworthy, several GIA models currently exist such as the ICE-3G (Tushingham and Peltier 1991) and the ICE-4G (Peltier 1994). However, we used the recent model proposed by Geruo, Wahr, and Zhong (2013) due to its state of the art estimation ability of the global GIA effect. Its advantages relate to new results for compressible Earth, and it uses an elastic structure and viscosity profile with a continuously varying radius along the mantle, unlike older versions. To obtain the ellipsoidal uplift variations in the lithosphere from the model, a spherical harmonics expansion developed up to 60° and filtered with a Gaussian filter of 200 km was applied.

Furthermore, a trend was estimated using the simple linear regression model (SLRM) of sea level with respect to time to explore this discrepancy with the multivariable model. The difference in the two models' estimated trends expressed the aliasing of the inter-annual and decadal climate variability.

3. Results and discussions

3.1. Vertical deformation along the Chilean coast

The behaviour of the vertical deformations along the Chilean coast presented an important spatial variability. This can be explained by the interaction between the Nazca and South American plates and the set of segments that make up the crustal structures along the Chilean coast (see Table 6).

The independent estimates of the vertical motion of ALT-TG and GPS present a high consistency in the extreme stations, and important differences in the stations located in the central region. The vertical deformations obtained from ALT-TG and GPS showed agreement in the ARIC, IQUE, ANTO, SANO, CALD, ANCU, PTAR, and PWIL TGs with a correlation coefficient of 0.9, which is statistically significant at an alpha level of 0.05 (see Table 5). However, vertical deformation values from ALT-TG that show major disagreement compared to vertical motion by GPS are those associated with the VALP, CONZ, and PMON TGs (see Table 6).

The PMON TG is located in complex estuary morphological conditions where the sea level signal is influenced by the presence of islands, fiords and bays.

On the other hand, in regards to the TALC station, the disagreement between GPS and TG could be related to the high seismic activity and problems in the model while estimating the trend (e.g. modelling of the post-seismic effect and the associated period of time). The distance between the TG and the GPS station could also

be an element that introduces difference in the estimated trends (e.g. local effects associated with each station).

In addition, the trends estimated by ALT-TG show a high degree of dispersion, which can be seen in [Table 6](#).

Another aspect related to the differences of vertical deformation found between ALT-TG and GPS is that the GPS time span is shorter than that of the ALT-TG time series, since most of the GPS time series started in 2007 and ended in 2015. For this reason, the period of study for both datasets do not exactly match, which can lead to differences in the estimated vertical motions.

It should be noted that one of the most important limitations in determining the SLC from TG and GPS observations is the correct vertical deformation modelling from GPS in highly seismic regions such as Chile (e.g. to remove the co and post-seismic effect). For this reason, the satellite ALT can be considered a key tool in the study of SLC.

3.2. SLC along the Chilean coast

With regard to the estimate of SLC in the Chilean coast, slight differences between the estimates from SLRM and MVLR models were found (see [Table 7](#)). The differences could be associated with the annual and decadal effects. According to our results of the MVLR, sea level is increasing from 1.2 to 0.2 mm year^{-1} in most of the Chilean coast from north to south, with the exception of PTAR and PWIL TGs, where we found a decrease of -0.9 and $-0.8 \text{ mm year}^{-1}$, respectively (see [Table 7](#)). In other words, the change in sea level in Chile shows slight agreement with the global trend ($\sim 3 \text{ mm year}^{-1}$), estimated with satellite altimeters for at least three decades (Cazenave et al. 2014) with the exception of the southernmost part of Chile.

According to minor values indicated by the GIA model used herein, this effect represents a small contribution in the vertical deformation in the Chilean coast, reaching a maximum of 0.19 mm in the PMON and ANCU TGs.

On the other hand, the aliasing effect obtained from the different trends between the MVL and SLRM models reveals an important contribution of decadal and inter-decadal components, reaching up to 0.7 mm year^{-1} .

Table 7. Trend estimated by MVLR and SLR and aliasing.

Station	SLR		GIA (mm year^{-1})	MVLR		
	Trend (mm year^{-1})	Standard deviation (mm year^{-1})		Trend (mm year^{-1})	Std deviation (mm year^{-1})	Aliasing (mm year^{-1})
ARIC	0.53	0.14	-0.01	1.19	0.15	0.66
IQUI	0.39	0.13	0.02	0.97	0.14	0.58
ANTO	0.34	0.12	0.02	0.80	0.13	0.46
SANO	0.46	0.16	0.16	0.75	0.18	0.29
CALD	-0.17	0.15	0.10	0.20	0.16	0.36
VALP	0.43	0.16	0.16	0.73	0.18	0.30
TALC	0.04	0.20	0.18	0.40	0.21	0.35
PMON	0.39	0.18	0.19	0.63	0.20	0.24
ANCU	0.38	0.18	0.19	0.61	0.20	0.23
PTAR	-1.34	0.23	0.06	-0.91	0.25	0.43
PWIL	-1.27	0.25	0.01	-0.83	0.27	0.44

In our research, SLC between January 1994 and January 2015 was estimated from satellite ALT, and the annual, decadal, and inter-decadal effects were considered by the GIA. However, variations in sea level due to the high seismicity (major earthquakes) in Chile could cause slight variations that were not considered in this study (Melini and Piersanti 2006; Melini et al. 2004). Improvements in the accuracy of the altimeter sensor observations and improvements in the setting values for viscoelastic mantles are needed to improve the estimate of the change in sea level.

4. Conclusion

In this contribution, we presented an estimate of the vertical deformation of the Chilean coast through TGs and satellite ALT observations for a period of ~20 years. Our results reveal that the behaviour of the vertical deformations along the Chilean coast presents an important spatial variability. This can be explained by the interaction between the Nazca and South American plates and the set of segments that make up the crustal structures along the Chilean coast. Also, good consistency was found (correlation coefficient of 0.9) with vertical deformations obtained from GPS precise positioning in most stations (8 of 11 stations). The estimate of the SLC in the Chilean coast revealed an overall increase in sea level. The sea level in Chile does not strictly follow the global trend ($\sim 3 \text{ mm year}^{-1}$), but has a slight agreement (from 1.2 to 0.6 mm year^{-1}) from Arica to Puerto Montt, with the exception of PTAR and PWIL TGs, where we found a decrease of -0.9 and $-0.8 \text{ mm year}^{-1}$, respectively. Our results of vertical motion could contribute to the study of crustal deformation for longer periods than those obtained from GPS positioning, and our estimate of the SLC could provide evidence of a local phenomenon that is generating important difference with regard to global trends (e.g. ocean currents, thermal expansion, and glaciers in the south).

It should also be noted that the estimates of sea level from TGs and GPS data are considerably limited by the correct modelling of geodynamic effects involved in the signal of these sensors. Therefore, it is essential to continue exploring changes in sea level with satellite ALT.

We are working on future studies involving remote sensing missions like those related to the gravity field, as well as incorporating data from other sensors, e.g. sea surface temperature from the Moderate Resolution Imaging Spectroradiometer (MODIS) mission, to model the impact of the regional seismicity in the estimations of SLC in Chile.

Acknowledgements

The author Silvio De Freitas would like to thank the CNPq Process 306936/2015-1. Vagner G. Ferreira was partially supported by the National Natural Science Foundation of China (Grant No. 41574001). We thank Department of Earth Observation and Space Systems (DEOSs) of the Faculty of Aerospace Engineering, Technical University Delft for satellite altimetry (ALT) data access, and the Chilean Navy Hydrographic and Oceanographic Service – SHOA for providing the Tide Gauge sea level data. We also thank P. Wessel and W. H. F. Smith for the use of the GMT-mapping software.

Disclosure statement

The authors confirm no conflicts of interest.

Funding

The author Silvio De Freitas would like to thank the CNPq Process 306936/2015-1. Vagner G. Ferreira was partially supported by the National Natural Science Foundation of China [Grant No. 41574001].

References

- Bawden, G. W., W. Thatcher, R. S. Stein, K. W. Hudnut, and G. Peltzer. 2001. "Tectonic Contraction across Los Angeles after Removal of Groundwater Pumping Effects." *Nature* 412 (6849): 812–815. doi:10.1038/35090558.
- Beavan, J., P. Denys, M. Denham, B. Hager, T. Herring, and P. Molnar. 2010. "Distribution of Present-Day Vertical Deformation across the Southern Alps, New Zealand, from 10 Years of GPS Data." *Geophysical Research Letters* 37 (16): n/a-n/a. doi:10.1029/2010GL044165.
- Bevis, M., and A. Brown. 2014. "Trajectory Models and Reference Frames for Crustal Motion Geodesy." *Journal of Geodesy* 88 (3): 283–311. doi:10.1007/s00190-013-0685-5.
- Blewitt, G. 2007. "GPS and Space-Based Geodetic Methods." In *Treatise on Geophysics*, edited by Tom Herring, Vol. 3, 351–390. Cambridge, MA: Massachusetts Institute of Technology. doi:10.1016/B978-044452748-6.00058-4.
- Cazenave, A., K. Dominh, F. Ponchaut, L. Soudarin, J. F. Cretaux, and C. Le Provost. 1999. "Sea Level Changes from Topex-Poseidon Altimetry and Tide Gauges, and Vertical Crustal Motions from DORIS." *Geophysical Research Letters* 26 (14): 2077–2080. doi:10.1029/1999GL900472.
- Cazenave, A., and R. S. Nerem. 2004. "Present-Day Sea Level Change: Observations and Causes." *Reviews of Geophysics* 42 (3): 1–20. doi:10.1029/2003rg000139.
- Cazenave, A., H.-B. Dieng, B. Meyssignac, K. Von Schuckmann, B. Decharme, and E. Berthier. 2014. "The Rate of Sea-Level Rise." *Nature Climate Change* 4 (5): 358–361. doi:10.1038/nclimate2159.
- Church, J. A., T. Aarup, L. P. Woodworth, S. W. Wilson, J. R. Nicholls, R. Rayner, K. Lambeck, et al. 2010. "Sea-Level Rise and Variability: Synthesis and Outlook for the Future." In *Understanding Sea-Level Rise and Variability*, edited by J. A. Church, P. L. Woodworth, T. Aarup, and W. S. Wilson, 402–419. Wiley-Blackwell. doi:10.1002/9781444323276.ch13.
- Church, J. A., P. U. Clark, A. Cazenave, J. M. Gregory, S. Jevrejeva, A. Levermann, M. A. Merrifield, et al. 2013. "Sea Level Change." *Climate Change 2013: The Physical Science Basis. Contribution of Working Group I to the Fifth Assessment Report of the Intergovernmental Panel on Climate Change*, 1137–1216. doi:10.1017/CB09781107415315.026.
- Dalla Via, G., M. Crosetto, and B. Crippa. 2012. "Resolving Vertical and East-West Horizontal Motion from Differential Interferometric Synthetic Aperture Radar: The L'Aquila Earthquake." *Journal of Geophysical Research: Solid Earth* 117 (2): 1–14. doi:10.1029/2011JB008689.
- DEOS. 2015. Radar Altimetry Database System. <http://rads.tudelft.nl/rads/rads.shtml>.
- Drewes, H., and O. Heidbach. 2012. "The 2009 Horizontal Velocity Field for South America and the Caribbean." In *Geodesy for Planet Earth SE - 81*, edited by S. Kenyon, M. C. Pacino, and U. Marti, edited by S. Kenyon, M. C. Pacino, and U. Marti, Vol. 136, 657–664. International Association of Geodesy Symposia. Springer Berlin Heidelberg. doi:10.1007/978-3-642-20338-1_81.
- Fenoglio-Marc, L., C. Dietz, and E. Groten. 2004. "Vertical Land Motion in the Mediterranean Sea from Altimetry and Tide Gauge Stations." *Marine Geodesy* 27: 683–701. doi:10.1080/01490410490883441.
- García, F., M. I. Vigo, D. García-García, and J. M. Sánchez-Reales. 2012. "Combination of Multisatellite Altimetry and Tide Gauge Data for Determining Vertical Crustal Movements

- along Northern Mediterranean Coast." *Pure and Applied Geophysics* 169 (8): 1411–1423. doi:10.1007/s00024-011-0400-5.
- Geruo, A., J. Wahr, and S. Zhong. 2013. "Computations of the Viscoelastic Response of a 3-D Compressible Earth to Surface Loading: An Application to Glacial Isostatic Adjustment in Antarctica and Canada." *Geophysical Journal International* 192 (2): 557–572. doi:10.1093/gji/ggs030.
- Gusman, A. R., S. Murotani, K. Satake, M. Heidarzadeh, E. Gunawan, S. Watada, and B. Schurr. 2015. "Fault Slip Distribution of the 2014 Iquique, Chile, Earthquake Estimated from Ocean-Wide Tsunami Waveforms and GPS Data." *Geophysical Research Letters* 42 (4): 1053–1060. doi:10.1002/2014GL062604.
- Larson, K. M., and V. D. Tonie. 2000. "Measuring Postglacial Rebound with GPS and Absolute Gravity." *Geophysical Research Letters* 27 (23): 3925–3928. doi:10.1029/2000GL011946.
- Lombard, A., A. Cazenave, P. Y. Le Traon, and M. Ishii. 2005. "Contribution of Thermal Expansion to Present-Day Sea-Level Change Revisited." *Global and Planetary Change* 47: 1–6. doi:10.1016/j.gloplacha.2004.11.016.
- Melini, D., and A. Piersanti. 2006. "Impact of Global Seismicity on Sea Level Change Assessment." *Journal of Geophysical Research* 111 (B3): B03406. doi:10.1029/2004JB003476.
- Melini, D., A. Piersanti, G. Spada, G. Soldati, E. Casarotti, and E. Boschi. 2004. "Earthquakes and Relative Sealevel Changes." *Geophysical Research Letters* 31 (9): 1–4. doi:10.1029/2003GL019347.
- Milne, G. A., J. L. Davis, J. X. Mitrovica, H. G. Scherneck, J. M. Johansson, M. Vermeer, and H. Koivula. 2001. "Space-Geodetic Constraints on Glacial Isostatic Adjustment in Fennoscandia." *Science (New York, N.Y.)* 291 (5512): 2381–2385. doi:10.1126/science.1057022.
- Nerem, R. S. 2002. "Estimates of Vertical Crustal Motion Derived from Differences of TOPEX/POSEIDON and Tide Gauge Sea Level Measurements." *Geophysical Research Letters* 29: 40-1-40-4. doi:10.1029/2002GL015037.
- Nerem, R. S., D. P. Chambers, C. Choe, and G. T. Mitchum. 2010. "Estimating Mean Sea Level Change from the TOPEX and Jason Altimeter Missions." *Marine Geodesy* 33 (sup1): 435–446. doi:10.1080/01490419.2010.491031.
- Niell, A. E. 1996. "Global Mapping Functions for the Atmosphere Delay at Radio Wavelengths." *Journal of Geophysical Research* 101: 3227–3246. doi:10.1029/95JB03048.
- Noomen, R., T. A. Springer, B. A. C. Ambrosius, K. Herzberger, D. C. Kuijper, G. J. Mets, B. Overgaauw, and K. F. Wakker. 1996. "Crustal Deformations in the Mediterranean Area Computed from SLR and GPS Observations." *Journal of Geodynamics* 21 (1): 73–96. doi:10.1016/0264-3707(95)00015-1.
- Pavlis, N. K., S. A. Holmes, S. C. Kenyon, and J. K. Factor. 2012. "The Development and Evaluation of the Earth Gravitational Model 2008 (EGM2008)." *Journal of Geophysical Research: Solid Earth* 117 (B4): n/a – n/a. doi:10.1029/2011JB008916.
- Peltier, W. R. 1994. "Ice Age Paleotopography." *Science (New York, N.Y.)* 265 (5169): 195–201. doi:10.1126/science.265.5169.195.
- Prandi, P., A. Cazenave, and M. Becker. 2009. "Is Coastal Mean Sea Level Rising Faster than the Global Mean? A Comparison between Tide Gauges and Satellite Altimetry over 1993–2007." *Geophysical Research Letters* 36 (5): L05602. doi:10.1029/2008GL036564.
- Reischung, P., J. Griffiths, J. Ray, R. Schmid, X. Collilieux, and B. Garayt. 2012. "IGS08: The IGS Realization of ITRF2008." *GPS Solutions* 16 (4): 483–494. doi:10.1007/s10291-011-0248-2.
- Sánchez, L., and H. Drewes. 2016. "Crustal Deformation and Surface Kinematics after the 2010 Earthquakes in Latin America." *Journal of Geodynamics* 102: 1–23. doi:10.1016/j.jog.2016.06.005.
- Schmid, R., P. Steigenberger, G. Gendt, G. Maorong, and M. Rothacher. 2007. "Generation of a Consistent Absolute Phase-Center Correction Model for GPS Receiver and Satellite Antennas." *Journal of Geodesy* 81 (12): 781–798. doi:10.1007/s00190-007-0148-y.
- Snay, R., M. Cline, W. Dillinger, R. Foote, S. Hilla, W. Kass, J. Ray, J. Rohde, G. Sella, and T. Soler. 2007. "Using Global Positioning System-Derived Crustal Velocities to Estimate Rates of Absolute Sea

- Level Change from North American Tide Gauge Records." *Journal of Geophysical Research: Solid Earth* 112: 4. doi:[10.1029/2006JB004606](https://doi.org/10.1029/2006JB004606).
- Soudarin, L., J. Crétaux, and A. Cazenave. 1999. "Vertical Crustal Motions from the DORIS Space-Geodesy System." *Geophysical Research Letters* 26: 1207–1210. doi:[10.1029/1999GL900215](https://doi.org/10.1029/1999GL900215).
- Sturkell, E., P. Einarsson, F. Sigmundsson, H. Geirsson, H. Ólafsson, R. Pedersen, E. D. Z.-V. Dalfsen, A. T. Linde, S. I. Sacks, and R. Stefánsson. 2006. "Volcano Geodesy and Magma Dynamics in Iceland." *Journal of Volcanology and Geothermal Research* 150 (1–3): 14–34. doi:[10.1016/j.jvolgeores.2005.07.010](https://doi.org/10.1016/j.jvolgeores.2005.07.010).
- Tesmer, V., P. Steigenberger, M. Rothacher, J. Boehm, and B. Meisel. 2009. "Annual Deformation Signals from Homogeneously Reprocessed VLBI and GPS Height Time Series." *Journal of Geodesy* 83 (10): 973–988. doi:[10.1007/s00190-009-0316-3](https://doi.org/10.1007/s00190-009-0316-3).
- Tushingham, A. M., and W. R. Peltier. 1991. "Ice-3G: A New Global Model of Late Pleistocene Deglaciation Based upon Geophysical Predictions of Post-Glacial Relative Sea Level Change." *Journal of Geophysical Research* 96: 4497–4523. doi:[10.1029/90JB01583](https://doi.org/10.1029/90JB01583).
- Vigny, C., A. Socquet, S. Peyrat, J.-C. Ruegg, M. Métois, R. Madariaga, S. Morvan, et al. 2011. "The 2010 Mw 8.8 Maule Megathrust Earthquake of Central Chile, Monitored by GPS." *Science (New York, N.Y.)* 332 (6036): 1417–1421. doi:[10.1126/science.1204132](https://doi.org/10.1126/science.1204132).
- Wahr, J., M. Molenaar, and F. Bryan. 1998. "Time Variability of the Earth's Gravity Field: Hydrological and Oceanic Effects and Their Possible Detection Using GRACE." *Journal of Geophysical Research* 103: 30205–30229. doi:[10.1029/98JB02844](https://doi.org/10.1029/98JB02844).
- Watt, S. F. L., D. M. Pyle, and T. A. Mather. 2009. "The Influence of Great Earthquakes on Volcanic Eruption Rate along the Chilean Subduction Zone." *Earth and Planetary Science Letters* 277 (3–4): 399–407. doi:[10.1016/j.epsl.2008.11.005](https://doi.org/10.1016/j.epsl.2008.11.005).
- Wolter, K., and M. S. Timlin. 1998. "Measuring the Strength of ENSO Events: How Does 1997/98 Rank?." *Weather* 53: 315–324. doi:[10.1002/j.1477-8696.1998.tb06408.x](https://doi.org/10.1002/j.1477-8696.1998.tb06408.x).
- Zhang, X., and J. A. Church. 2012. "Sea Level Trends, Interannual and Decadal Variability in the Pacific Ocean." *Geophysical Research Letters* 39 (21): 1–8. doi:[10.1029/2012GL053240](https://doi.org/10.1029/2012GL053240).